JOURNAL OF THE KOREAN ASTRONOMICAL SOCIETY
34: 157 ~ 166, 2001

CO STUDY OF THE H II REGION SHARPLESS 301

JAE HOON JUNG[1], JUNG-KYU LEE[2,4], TAE SEOG YOON[2], AND YONG HEE KANG[3]
[1]Korea Astronomy Observatory, Taejeon 305-348, Korea
[2]Department of Astronomy and Atmospheric Sciences, Kyungpook National University, 702-701, Korea
[3]Department of Earth Science Education, Kyungpook National University, 702-701, Korea
[4]School of Physics, University of New South Wales, Sydney 2052, Australia
E-mail: jhjung@trao.re.kr
(Received Oct. 17, 2001; Accepted Nov. 1, 2001)

ABSTRACT

The molecular cloud associated with the H II region S301 has been mapped in the $J = 1-0$ transitions of ^{12}CO and ^{13}CO using the 13.7 m radio telescope of Taeduk Radio Astronomy Observatory. The cloud is elongated along the north-south direction with two strong emission components facing the H II region. Its total mass is 8.7×10^3 $M_\odot$. We find a velocity gradient of the molecular gas near the interface with the optical H II region, which may be a signature of interaction between the molecular cloud and the H II region. Spectra of CO, CS, and HCO^+ exhibit line splitting even in the densest part of the cloud and suggests the clumpy structure. The radio continuum maps show that the ionzed gas is distributed with some asymmetry and the eastern part of the H II region is obscured by the molecular cloud. We propose that the S301 H II region is at the late stage of the champagne phase, but the second generation of stars has not yet been formed in the postshock layer.

Key words : H II region — ISM: individual (S301) — ISM: molecular lines — ISM: morphology

I. INTRODUCTION

H II regions located near the edge of molecular clouds consist of ionized gas which is expanding asymmetrically (Israel 1978). These asymmetric flows have been interpreted with the blister or champagne models (Israel 1978; Tenorio-Tagle 1979). A blister-type H II region is ionization-bound on the molecular cloud side and density-bound on the other side, and appears asymmetric. Many observational examples of the blister (Mufson et al. 1981; Joncas & Roy 1984, 1986; Joncas, Durand, & Roger 1992; Miville-Deschênes, Joncas, & Durand 1995) have been found, and also their evolutions are relatively well studied theoretically by many authors (see the review of Yorke 1986 and references therein).

The H II region S301 [α_{1950}= $7^h07^m41.9^s$, δ_{1950}= $-18°25'25''$] (Brand, Blitz, & Wouterloot 1986) is located at the edge of a molecular cloud. It looks like a well defined optical H II region on the blue print of POSS, but shows an extended weak nebulosity in the opposite direction of its parent cloud on the red print. The principal exciting star is barely seen at the edge of the optical H II region and has been classified as an O7 star by Moffat, Fitzgerald, & Jackson (1979). There exists a velocity difference of $\sim$ 3.5 km s^{-1} between the molecular cloud and the ionized gas (Wouterloot & Brand 1989; Fich, Treffers, & Dahl 1990; Fich & Silkey 1991). Thus S301 is a good candidate for a blister.

To understand the interaction between H II region and molecular cloud, knowledge of the velocity fields of both molecular and ionized gases are essential. Until now , however, no systematic observations have been made of S301. A partial CO mapping (Jackson & Sewall 1982) and H_2O maser search (Wouterloot, Brand, & Henkel 1988) were performed. Moffat et al. (1979) and Brand & Blitz (1993) derived a distance of 5.8 and 4.23 kpc to it from photometry, respectively. Shaver et al. (1983) and Wouterloot & Brand (1989) derived the kinematic distance of 4.3 and 5.3 kpc from the hydrogen recombination line and CO observations, respectively. We adopt the arithmetic mean distance of 5 ± 1 kpc (Jung, Koo, & Kang 1996), which implies that S301 lies in the Perseus arm.

We made CO observations of the S301 molecular cloud to examine the distribution of molecular gas and the velocity structure. These observational results were analyzed and compared with radio continuum observations to understand the relationship between the molecular cloud and the optical H II region. The observational methods are described in Section II. In Section III, the spatial distribution and the velocity structure of CO emission are described and the related physical parameters are derived. We discuss the morphology and the star formation in Section IV, and summarize our results briefly in Section V.

II. OBSERVATIONS

Observations of the $J = 1-0$ transition of ^{12}CO and ^{13}CO were performed using the Taeduk Radio Astronomy Observatory (TRAO) 13.7m telescope (HPBW=44″ at 115 GHz) in May and October 1994, and February 1995. A cooled Schottky diode mixer receiver equiped with a quasi-optical sideband filter was used along with

two 256 channel filterbanks of a 250 kHz frequency resolution. The main beam efficiency was 0.47 at 115 GHz (Kim & Jung 1992), and the pointing accuracy was better than 10″. During the observations, Orion KL, as a calibration source, was observed every day to check the stability of the system. No significant changes in line intensities were found. Typical system temperatures were about 1600 K (SSB) at 115 GHz and 900 K (SSB) at 110 GHz, which were obtained by the standard chopper wheel method of Ulich & Haas (1976). Mapping was made in position-switching mode centered at (α_{1950}, δ_{1950})=($7^h08^m, -18°24'$), near IRAS 07080-1824. The areas observed in ^{12}CO and ^{13}CO are $24' \times 42'$ and $14' \times 28'$, respectively. These observations were made with different spacings; 1′ in dense regions ($\Delta\delta > -12'$) and 1.′5 in weak emission regions of the southern ridge. The rms noise antenna temperatures are less than 0.25 K and 0.15 K in T_A^* for ^{12}CO and ^{13}CO, respectively.

In April 1998 we also made supplementary observations of high density tracers, HCO^+ ($J = 1 - 0$), CS ($J = 2 - 1$), HCN ($J = 1 - 0$), and SiO ($J = 2 - 1, v = 0$), to confirm the velocity structure. We used an SIS receiver with a typical system temperature of 800 K at 115 GHz, and a 1024 channel autocorrelator of a total bandwidth 20 MHz.

III. RESULTS OF CO OBSERVATIONS

(a) Distribution of Molecular Gas

Fig. 1 shows the integrated intensity maps of ^{12}CO and ^{13}CO. The velocity ranges of the integrated intensity maps are 48 – 58 km s^{-1} for ^{12}CO, and 49 – 56 km s^{-1} for ^{13}CO. The cloud is elongated along a north-south direction. The total extent of the S301 molecular cloud is $15' \times 38'$ or 22×55 pc at a distance of 5 kpc. Two strong emission regions centered at the offset positions, $(0', 0')$ and $(-6', -7')$, appear adjacent to the optical H II region (see Fig. 5d). The northeastern (NE) component is compact and round, while the southwestern (SW) one is embedded in a diffuse emission region extended over a much larger area to the south. They are connected by rather weak emission near the principal exciting star, and the optical H II region is located at the edges of the two components, nearly intervening between them. This suggests that the dissociation of molecular gas may have occurred on this side.

The ^{13}CO integrated intensity map (Fig. 1b) shows that these two components have a clumpy structure. However, the clumps are not clearly resolved due to the poor spatial resolution of our observations. Our mapping grid (1′) corresponds to 1.5 pc at a distance of 5 kpc, which is larger than the size of massive star forming cores, ~1 pc (Harju, Walmsley, & Wouterloot 1993). In the SW component, the ^{13}CO emission forms a shell-like structure of 8′ diameter centered at offset $(-4', -8')$. The position-velocity diagrams across the shell, however, do not show any evidence for an expanding shell. Moreover, the IRAS point source IRAS 07075−1831 (open circle in Fig. 1b) located near the center of the shell was identified as an external galaxy (Saito et al. 1991; Weinberger, Sauer, & Seeberger 1995).

(b) Velocity Structure

Channel maps of ^{12}CO and ^{13}CO emissions are displayed in Fig. 2. The strongest emission comes from the NE and the SW components. The clumpy structure appears even in ^{12}CO, and each clump has a slightly different ($\lesssim 2$ km s^{-1}) velocity. Fig. 2 also shows that the line intensity decreases more rapidly toward the optical H II region, especially in the SW component and a higher velocity component appears near the H II region interface, which suggest an interaction between the molecular cloud and the ionized gas. The two velocity components (see below) observed in the NE component may also support the interaction. We assume that both the NE and the SW components are disturbed by the H II region, and adopt v_{LSR}= 52 km s^{-1} as the systemic velocity of the S301 molecular cloud where the largest molecular structure appears. This velocity is not much different from that of the ionized gas measured by radio recombination lines (v_{LSR}= 55.5 km s^{-1}; Fich & Silkey 1991), and suggests that the optical H II region is physically associated with the observed molecular cloud.

To see the velocity structure of the disturbed layer, position-velocity diagrams of ^{12}CO are plotted in Fig. 3, which are made from the autocorrelator data. Figs. 3a and 3b are the north-south strip ($\Delta\alpha = -6'$) and the east-west strip ($\Delta\delta = -2'$), respectively. These directions are orthogonal to the ionization front (IF), and could show the velocity structure across the IF effectively. Note that there is no systematic change in the line width, but a velocity gradient appears in both strips. Especially, the north-south strip (Fig. 3a) shows that the peak velocity decreases systematically from the edge to the center of the SW component. In the east-west strip (Fig. 3b), however, a low-velocity component is found to be close to the exciting star. Since the east-west strip crosses the weak emission region and can not represent the velocity structure of the NE component, we present a north-south strip crossing the center ($\Delta\alpha = 0'$) of the NE component in Fig. 3c to confirm the velocity structure of the central part of the NE component. It also shows that the peak velocity is red-shifted even in the central part of the NE component. These could be interpreted that the NE component as a whole is disturbed by the H II region, but only the edge of the SW component is disturbed.

Fig. 3c suggests that the spectrum is made up of two velocity components: a weak blue one near v_{LSR}~ 51.5 km s^{-1} and a strong red one near v_{LSR}~ 53.5 km s^{-1} (see also Fig. 4a). The two components feature was also confirmed in the high density tracers as shown in Fig. 4. The line profiles were taken at the offset position

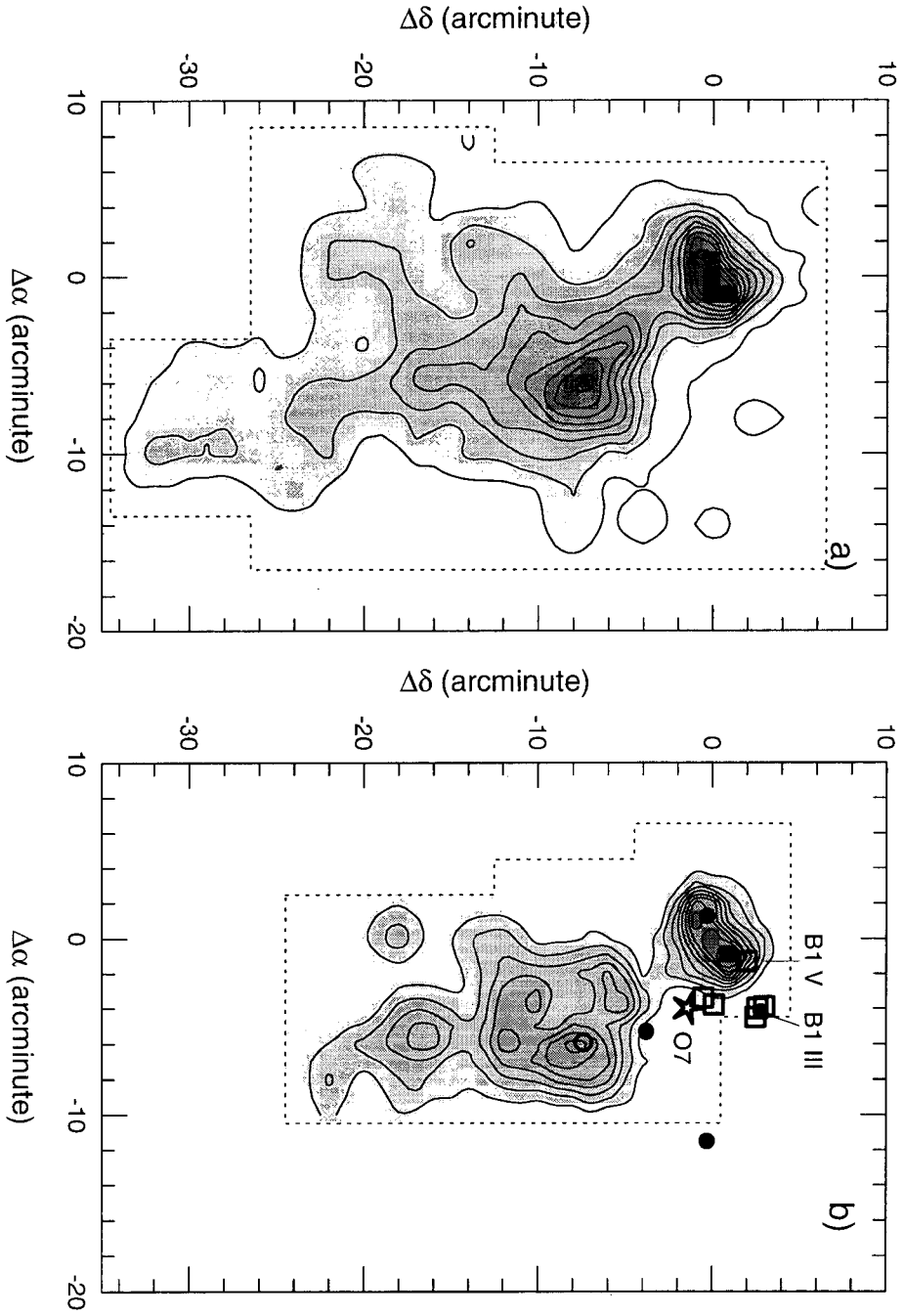

Fig. 1.— (a) ^{12}CO integrated intensity map in the velocity range from 48 to 58 km s^{-1}. The lowest contour is 1 K km s^{-1}, and the contour interval is 2 K km s^{-1}. (b) ^{13}CO integrated intensity map in the velocity range from 49 to 56 km s^{-1}. The lowest contour is 0.5 K km s^{-1}, and the contour interval is 0.4 K km s^{-1}. IRAS point sources and the exciting stars (Moffat et al. 1979) are also presented as filled circles and open squares, respectively. The principal exciting star, O7, is denoted as an asterisk.

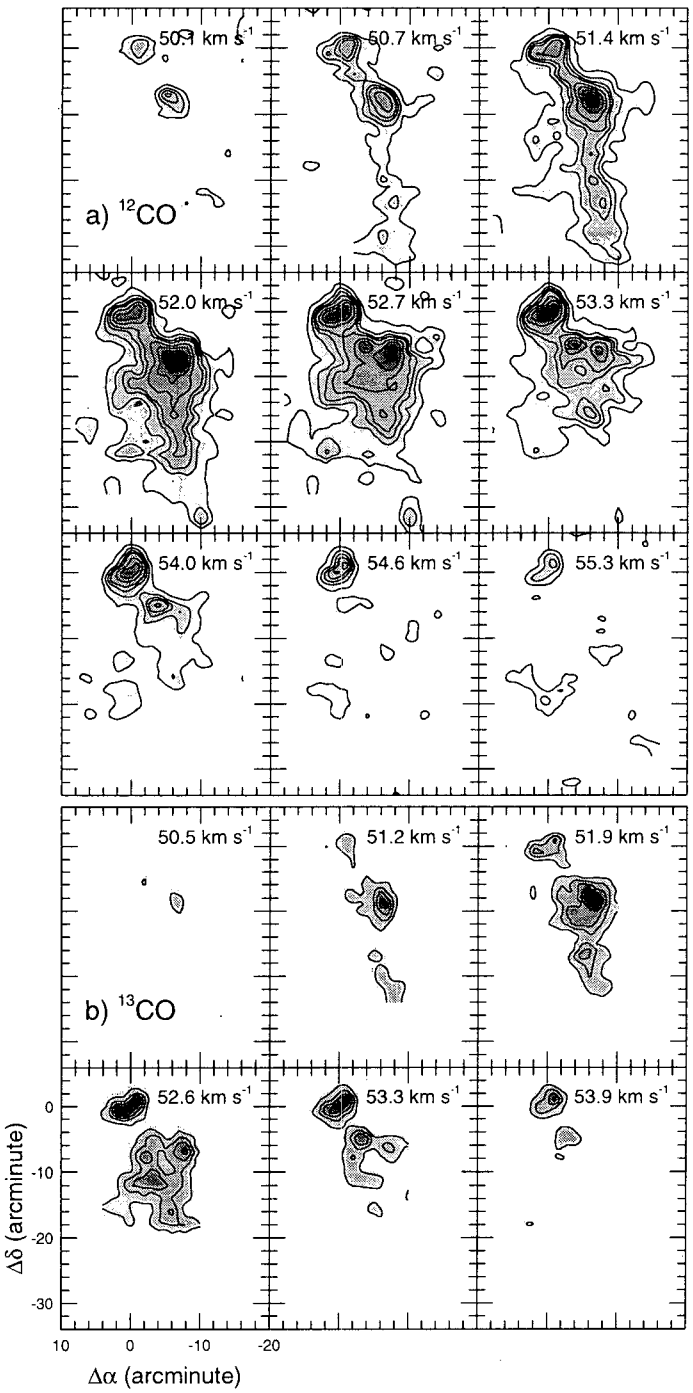

Fig. 2.— (a) ^{12}CO antenna temperature channel maps with a velocity interval of 0.65 km s^{-1}. The lower contour starts form 0.5 K with 0.5 K interval and the higher one starts from 3 K with 1 K interval. (b) ^{13}CO channel maps with a velocity interval of 0.68 km s^{-1}. The lowest contour is 0.3 K, and the contour interval is 0.3 K. Central velocities are labeled on top of the pictures.

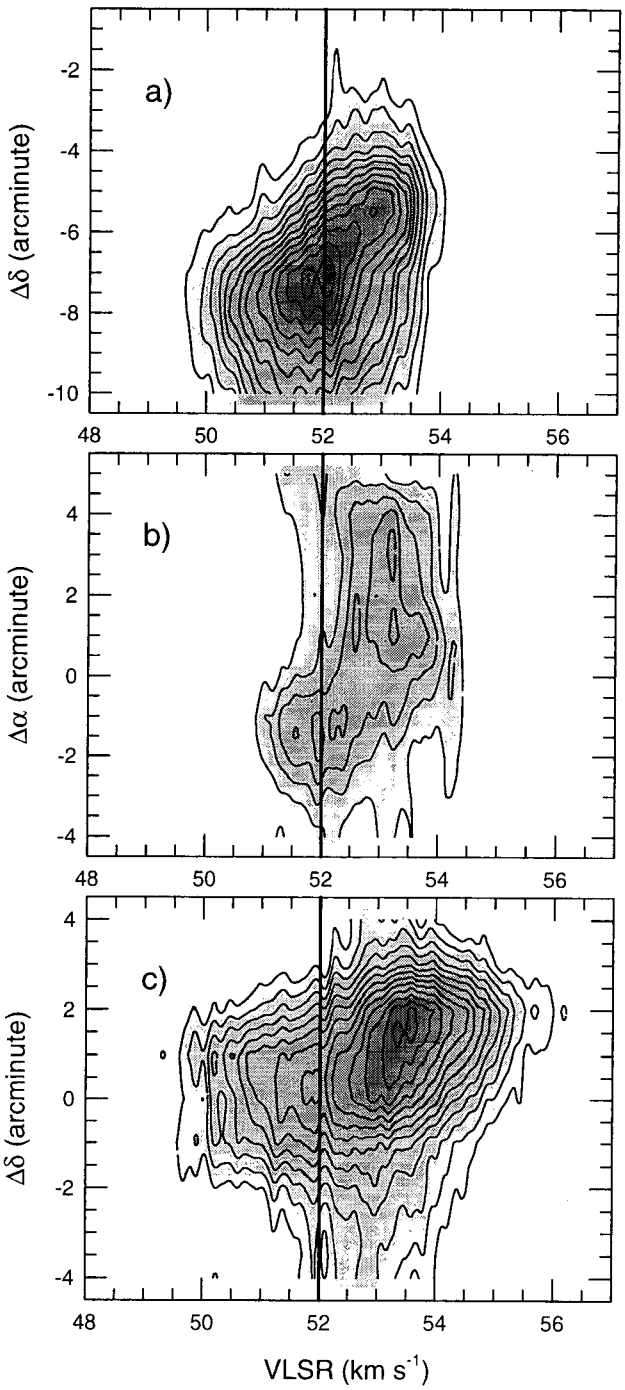

Fig.3.— Position-velocity diagrams with the autocorrelator data. The contour starts from 0.7 K with 0.5 K interval. The vertical lines at $v_{\rm LSR}$= 52.0 km s^{-1} represent the systemic velocity of the cloud. (a) North-south strip crossing the SW component ($\Delta\alpha = -6'$). (b) East-west strip crossing the principal exciting star ($\Delta\delta = -2'$). (c) North-south strip crossing the center of the NE component ($\Delta\alpha = 0'$).

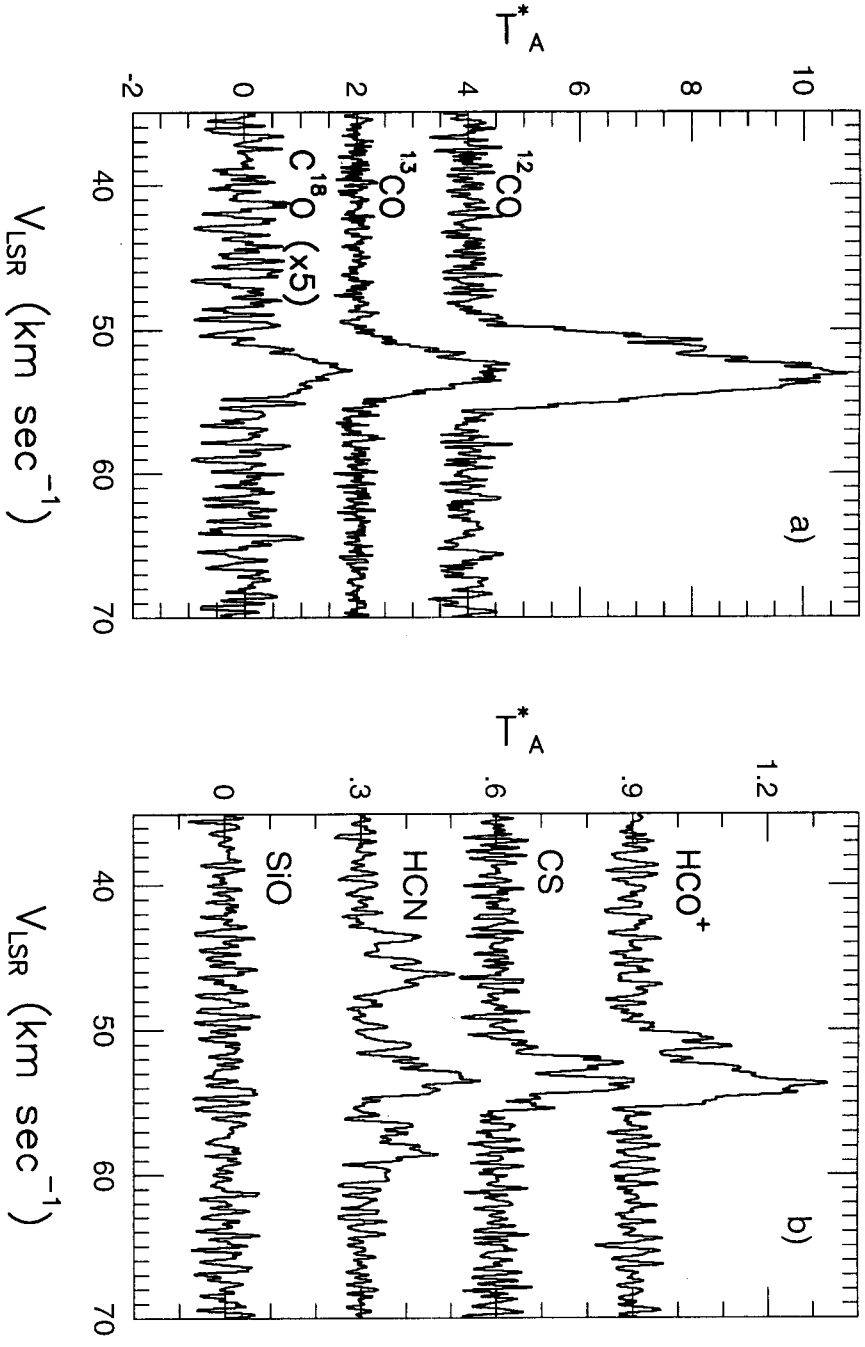

Fig. 4.— Observed line profiles at $(-1', 1')$ offset position where ^{13}CO intensity is strongest. (a) $J = 1 - 0$ lines of ^{12}CO and its isotope variants. (b) HCO^+ ($J = 1 - 0$), CS ($J = 2 - 1$), HCN ($J = 1 - 0$), and SiO ($J = 2 - 1, v = 0$) lines.

of $(-1', 1')$ where the intensity of ^{13}CO was strongest. The velocity difference between the two components is about 2 km s^{-1}. The lines from the high density tracers are weak but of similar intensity, about 0.3 K. Their optical depths are less than 0.05, if LTE is assumed, while that of ^{13}CO is appreciable, $\tau_{^{13}CO} = 0.45$. Because the components near 51.5 and 53.5 km s^{-1} can be seen in low (HCO^+) and high (^{12}CO) optical depth transitions the line splitting is due to overlap rather than self-absorption. Although we could not resolve the clumps in our observations, several velocity components observed in our observations of CO, HCO^+, and CS, suggest the clumpiness of the cloud. The blue asymmetry of the CO line profile observed by Wouterloot & Brand (1989) also can be explained by overlap.

(c) Mass of Cloud

In LTE, the ^{13}CO column density ($N_{^{13}CO}$) is given by

$$N_{^{13}CO} = \frac{2.42 \times 10^{14} \Delta V_{^{13}CO} T_{ex} \tau^{13}}{1 - \exp[-5.29/T_{ex}]} \quad \text{cm}^{-2} \quad (1)$$

where $\Delta V_{^{13}CO}$ is the full width at half intensity in km s^{-1}, τ^{13} is the linecenter optical depth of ^{13}CO, and T_{ex} is the excitation temperature. By assuming that the ^{12}CO line is optically thick, we derive T_{ex} from the peak ^{12}CO radiation temperature (T_R^{12}) and the column density using equation (1) *pixel by pixel.* For pixels weaker than the 3σ noise level or with no ^{13}CO data, the column densities were obtained from the ^{12}CO integrated intensity (W_{CO}) using the relation derived *in this study,*

$$N_{H_2} = 1.0 \times 10^{20} \times W_{CO}[\text{K km s}^{-1}] \quad \text{cm}^{-2} \quad (2)$$

where N_{H_2} is the column density of hydrogen molecules. The conversion factor is not much different from that determined by Strong & Mattox (1996), 1.9×10^{20}. The abundance ratio of H_2 to ^{13}CO is adopted to be 5×10^5 (Dickman 1978), and the distance to the cloud is assumed to be 5 kpc (see § 1). The derived molecular masses (including helium) are 1.9×10^3 $M_\odot$ and 3.2×10^3 $M_\odot$ for the NE and SW components, respectively. The total mass of the S301 molecular cloud including the southern diffuse region is 8.7×10^3 $M_\odot$.

We also derived the virial masses for the NE and the SW component with the following equation,

$$M_{VIR} = \frac{5\sigma_{tot}^2}{2G} D \quad (3)$$

where D is a diameter, G is a gravitational constant. σ_{tot} is the one dimensional velocity dispersion which corresponds to the square root sum of centroid velocity dispersion (σ_c) and internal velocity dispersion (σ_i) ($\sqrt{\sigma_i^2 + \sigma_c^2}$). Here, we assumed a uniform density distribution and a spherical cloud. The derived virial masses of the NE and SW components are 1.4×10^4 and 9.1×10^3 $M_\odot$, respectively. These values are about 7 times larger for the NE component and 3 times larger for the SW component than those derived from LTE analysis. This result implies that at least the NE component is likely to be disturbed by the H II region.

IV. DISCUSSION

(a) Morphology and Evolution

The optical H II region S301 is located at the northwestern edge of the molecular cloud. In the red print of POSS (Fig. 5d), it appears nonspherical due to the overlap of two nebulae: LBN 1044, a bright nebula on the cloud side and LBN 1043, a diffuse nebula on the other side. The optical brightness distribution is a reminiscent of an edge-on champagne flow (Tenorio-Tagle 1979). LBN 1043 and LBN 1044 may correspond to the density-bound and the ionization-bound region, respectively. The principal exciting star is barely seen ($E_{B-V} = 0.76$: Moffat, Fitzgerald, & Jackson 1979) at the interface between the optical H II region and its parent cloud (see Fig. 1b). The lowest CO contour forms a half circle at the interface, suggesting that the evaporation of molecular cloud is still going on.

In order to examine the distribution of the ionized gas, the 21 cm (NVSS; Condon et al. 1998), 11 cm (Fürst, Reich, & Reif 1990), and 6 cm (Condon, Broderick, & Seielstad 1991) continuum maps are reproduced in Fig. 5. The HPBWs of each observation are 45″, 4.′3, and 7′, and the pixel sizes are 15″, 2′, and 1.′7, respectively. The 21 cm NVSS and the 6 cm survey data were from Skyview. We also present the POSS red print together with the ^{12}CO integrated intensity map in Fig. 5d. The continuum maps show that the ionized gas is distributed with some asymmetry, although the 21 cm map shows only the bright region because of the larger size of S301 than 10′(Fich 1993). The emission peak of continuum map is shifted $\sim$ 1.′5 to the cloud side from the principal exciting star (see Fig 5a). These agree well with the theoretical edge-on morphology of a blister (Icke, Gatley, & Israel 1980; Yorke, Tenorio-Tagle, & Bodenheimer 1983) at radio wavelengths. However, Fig. 5 does not show a steep gradient of radio brightness to the molecular cloud, which appears in the theoretical radio continuum map (Yorke, Tenorio-Tagle, & Bodenheimer 1983) of edge-on morphology. Since the radio appearance of the champagne flow becomes more symmetric as the H II region evolves (Yorke, Tenorio-Tagle, & Bodenheimer 1983), this could be a result of the old age of the S301 H II region. The low electron density, $n_e \sim 18\text{cm}^{-3}$(Shaver et al. 1983; Fich & Silkey 1991) and the large dynamical age, $R/v_{exp} \sim 1 \times 10^6$ yr may be the indication of the old age. The radius (R) and the expansion velocity (v_{exp}) of the H II region are assumed to be 14.5 pc and 15 km s^{-1}, respectively.

There exists a velocity difference ($\Delta V(v_{CO} - v_{H_\alpha})$) ~ -3.5 km s^{-1} between CO and radio recombination

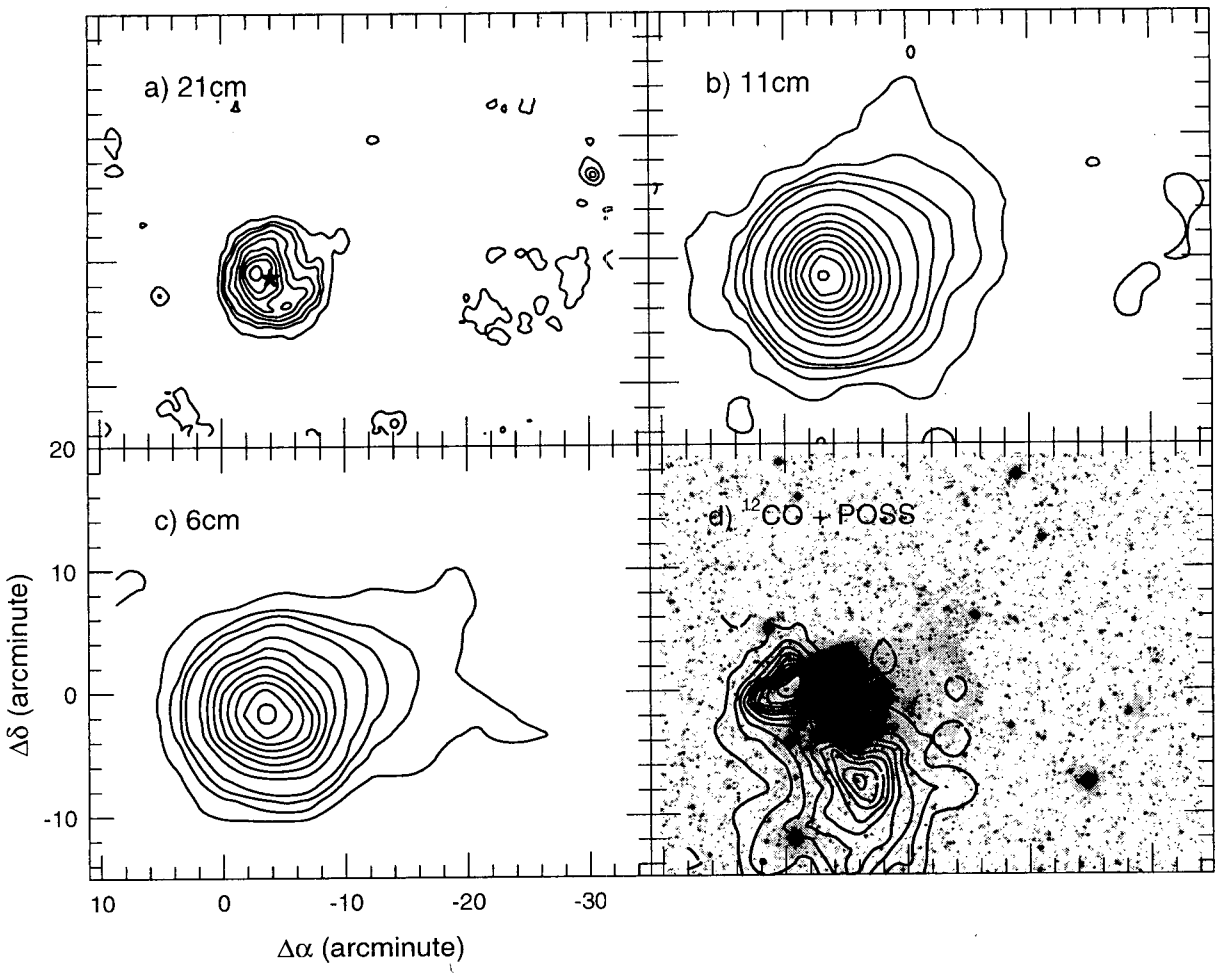

Fig. 5.— (a) 21 cm radio continuum map(NVSS). The principal exciting star is denoted by an asterisk. (b) 11 cm radio continuum map. (c) 6 cm radio continuum map. (d) The POSS red print superposed on the ^{12}CO integrated intensity map of Fig. 1a.

line (v_{LSR}= 55.5 km s^{-1}, FWHM=22 km s^{-1}: Fich et al. 1990) or H_α (v_{LSR}= 56.1 km s^{-1}, FWHM=33.3 km s^{-1}: Fich & Silkey 1991), which is nearly the same as the observed mean value for obscured blisters (Israel 1978). Fig. 5 also shows that the eastern part of H II region is obscured by the molecular cloud. Therefore, the S301 H II seems to be at the late stage of champagne phase and we are viewing it almost edge-on, slighly larger than 90°. However we could not explain the difference of peak velocity in both edges with any geometry. The velocity structure at the disturbed layer seems to be more related with the clumpy structure than the systematic motion.

(b) Star Formation

An isothermal shock (IS) is formed when the ionization front(IF) proceeds into the molecular cloud and a cooled, postshock (CPS) layer forms between IS and IF (Bedijn & Tenorio-Tagle 1981). The CPS layer will become gravitationally unstable and eventually form stars (Elmegreen & Lada 1977). In order to examine the star-forming activity, we plot all the exciting stars (Moffat, Fitzgerald, & Jackson 1979) and young star candidates (Emerson 1987) as open squares and filled circles, respectively in Fig. 1b. The principal exciting star, O7, which is overlapped with IRAS 07077-1825, is denoted by an asterisk. Most stars are located outside the ^{13}CO cloud, whereas the positions of IRAS point sources do not show any clear correlation with the ^{13}CO map. This implies that recent star formation may not proceed yet in the shocked layer. No detection of both maser sources (Wouterloot, Brand, & Henkel 1988) and the shock sensitive molecule, SiO (see Fig. 4) may also suggest no recent star formation.

There are two sources, a star (B1 V, E_{B-V} =0.47: Moffat, Fitzgerald, & Jackson 1979) and IRAS 07080-1824, near ^{13}CO cores of the NE component, which are young star or young star candidate associated with the

molecular cloud. Especially, IRAS 07080-1824 is possibly a young stellar object based on IRAS colors (Beichman et al. 1986; Emerson 1987; Walker et al. 1989), or possibly an embedded OB star candidate according to the classification of Wood & Churchwell (1989). The secondary peak of the dust temperature near IRAS 07080-1824 (Jung 1996) also suggests that IRAS 07080-1824 may be a heating source. However, it is uncertain whether they are the second generation formed by a sequential star forming mechanism. Near IR photometry could reveal additional embedded objects and could give some insights of the star forming mechanism.

V. SUMMARY

Extensive molecular line observations were performed for the molecular cloud associated with the optical H II region S301. The H II region is located at the edge of the cloud, and seems to be at the late stage of the champagne phase. The velocity structure of the molecular gas suggests that a ionization front might proceed into the parent cloud, but the star formation has not yet been triggered in the shocked layer. Our main results are the following.

(1) The parent molecular cloud of S301 extends over $\sim 15' \times 38'$ or 22×55 pc. The cloud is composed of two strong emission components facing the H II region and a ridge structure elongated along the north-south direction. The masses of the dense components are 1.9×10^3 and 3.2×10^3 $M_\odot$, respectively, and the total mass including the southern ridge is 8.7×10^3 $M_\odot$.

(2) Channel maps show that both high- and low-velocity components appear near the H II region interface, suggesting an interaction between the molecular and ionized gases. The velocity gradient apparent in the position-velocity map of the north-south strip (Fig. 3a) supports this idea. The big difference between the LTE and virial mass, at least for the NE component, may be the evidence of interaction between the molecular and ionized gases.

(3) The reversed velocity gradient appeared at the different edges of the cloud could not be explained with an expansion of the H II region. The velocity structure at the disturbed layer seems to be related with the clumpy structure rather than the systematic motion. The line splitting observed in low and high optical depth transitions also supports it.

(4) The H II region seems to be in the late stage of the champagne phase and we are viewing it almost edge-on, slightly larger than 90°. However, star formation might not be proceeded in the shocked layer yet, although a B1 V star and IRAS 07080-1824 near the ^{13}CO core are a young star and a young stellar object candidate.

This work was supported by the Research Fund of Kyungpook National University for the Selected Research Proposal of the year 1996. Part of this work was supported by grant R01-2000-0025 from the Basic Research Program of the Korea Science and Engineering Foundation(KOSEF).

REFERENCES

Bedijn, P. J. & Tenorio-Tagle, G. 1981, A&A, 98, 85

Beichman, C. A., Meyer, P. C., Emerson, J. P., Harris, S., Mathieu, R., Benson, P. J., & Jenning, R. E. 1986, ApJ, 307, 337

Brand, J., & Blitz, L. 1993, A&A, 275, 67

Brand, J., Blitz, L., & Wouterloot, J. G. A. 1986, A&AS, 65, 537

Condon, J. J., Broderick, J. J., & Seielstad, G. A. 1991, AJ, 102, 2041

Condon, J. J., Cotton, E. W., Perley, R. A., Taylor, G. B., & Broderick, J. J. 1998, AJ, 115, 1693

Dickman, R. L. 1978, ApJS, 37, 407

Elmegreen, B. G., & Lada, C. J. 1977, ApJ, 214, 725

Emerson, J. P. 1987, in Star Forming Reguions, IAU Symp. No. 115, eds. M. Peimbert and J. Jugaku (Dordrecht: Reidel), 19

Fich, M. 1993, ApJS, 86, 475

Fich, M., Treffers, R. R., & Dahl, G. P. 1990, AJ, 99, 622

Fich, M., & Silkey, M. 1991, ApJ, 366, 107

Fürst, E., Reich, W., & Reif, K. 1990, A&AS, 85, 691

Harju, J., Walmsley, C. M., & Wouterloot, J. G. A. 1993, A&AS, 98, 76

Icke, V., Gatley, I., & Israel, F. P. 1980, ApJ, 236, 808

Israel, F. P. 1978, A&A, 70, 769

Jackson, P. E. & Sewall, J. R. in Regions of Recent Star Formation, eds. R. S. Roger and P. E. Dewdney (Dordrecht: Reidel), 221

Joncas, G., Durand, D., & Roger, R. S. 1992, ApJ, 387, 591

Joncas, G., & Roy, J. R. 1984, ApJ, 283, 640

——————— 1986, ApJ, 307, 649

Jung, J. H. 1996, PhD thesis, Kyungpook National Univ.(Korea)

Jung, J. H., Koo, B-C, & Kang, Y-H 1996, AJ, 112, 1625

Kim, B. G., & Jung, J. H. 1992, PKAS, 7, 149

Miville-Deschênes, M.-A., Joncas, J., & Durand, D. 1995, ApJ, 454, 316

Moffat, A. F. G., Fitzgerald, M. P., & Jackson, P. D. 1979, ApJS, 38, 197

Mufson, S. L., Fountain, W. F., Gary, G. A., Howard, W. E., O'Dell, C. R., & Wolff, T. M. 1981, ApJ, 248, 992

Saito, M., Ohtani, H., Baba, A., Hotta, H., Kameno, S., Kurosu, S., Nakada, K., & Takata, T. 1991, PASJ, 43, 449

Shaver, R. A., McGee, R. X., Newton, L. M., Danks, L. C., & Pottasch, S. R. 1983, MNRAS, 204, 53

Strong, A. W., & Mattox, J. R. 1996, A&A, 308, L21

Tenorio-Tagle, G. 1979, A&A, 71, 59

Ulich, B. L., & Haas, R. W. 1976, ApJS, 30, 247

Walker, H. J., Cohen, M., Volk, K., Wainscoat, R. J., & Schwartz, D. E. 1989, AJ, 98, 2163

Weinberger, R., Sauer, W., & Seeberger, R. 1995, A&AS, 110, 269

Wood, D. O. S., & Churchwell, E_D 1989, ApJ, 340, 265

Wouterloot, J. G. A., & Brand, J. 1989, A&AS, 80, 149

Wouterloot, J. G. A., & Brand, J., & Henkel, C. 1988, A&A, 191, 323

Yorke, H. W. 1986, ARAA, 24, 49

Yorke, H. W., Tenorio-Tagle, G., & Bodenheimer, P. 1983, A&A, 127, 313